Electrochimica Acta 180 (2015) 460–470

Contents lists available at ScienceDirect

Electrochimica Acta

journal homepage: www.elsevier.com/locate/electacta

Carbon Supported Noble Metal (Pd and Au) Catalysts Synthesized by an Oxide Route with High Performance for Oxygen Reduction in Acidic Media

José L. Fernández[a,b,1], Kasun P. Imaduwage[a], Cynthia G. Zoski[a,*]

[a] Department of Chemistry and Biochemistry, New Mexico State University, Las Cruces, NM 88003, USA
[b] Programa de Electroquímica Aplicada e Ingeniería Electroquímica, Facultad de Ingeniería Química, Universidad Nacional del Litoral, Santa Fe, Argentina

ARTICLE INFO

Article history:
Received 3 July 2015
Received in revised form 6 August 2015
Accepted 7 August 2015
Available online 12 August 2015

Keywords:
Oxygen reduction
Metal oxide synthesis route
Electrocatalyst synergetic effects
Scanning electrochemical microscopy (SECM)
SECM activity screening

ABSTRACT

Carbon supported palladium (C/Pd) and gold (C/Au) catalysts were synthesized through a synthesis route involving oxide precipitation and partial reduction, and their performance for the oxygen reduction reaction (ORR) in acidic media was studied. Scanning electrochemical microscopy (SECM) ORR screening and tip-generation/substrate collection performed on glassy carbon supported metal spots showed a strong effect of the reactant ratio (precursor salt/precipitant/reducing agent) on the performance of the resulting catalysts for oxygen reduction and hydrogen peroxide production. These SECM results were further confirmed using a rotating ring-disk electrode with Nafion-embedded Vulcan carbon supported dispersed metal nanoparticles, and characterization with XRD and TGA. A significant enhancement in the overall activity for the ORR was observed on both C/Pd and C/Au catalysts under conditions involving metal oxide reduction, compared to those catalysts that were synthesized by direct metal salt reduction. For C/Pd, this enhanced overall activity with concomitant low peroxide yield is due to the different ways in which the metal and unreduced metal oxide in the catalysts interact with the hydrogen peroxide pathway. For C/Au, a highly dispersed metal with high electroactive area is obtained that shifts the potentials for the reduction of oxygen to hydrogen peroxide to near-reversible conditions.

1. Introduction

The overall catalytic activity of dispersed carbon supported materials for the oxygen reduction reaction (ORR) is dependent on a number of factors that include nature of the catalyst, particle size, degree of dispersion, and surface state of the catalyst, among others [1]. Mechanistic aspects that play key roles in the performance of a catalyst for the ORR include the dissociative adsorption of O_2 onto an active site, which is essential for the reaction to proceed via a 4-e^- pathway, and the simultaneous electrochemical reduction of oxygen to hydrogen peroxide, which decreases the faradaic efficiency for the 4-e^-reduction to water and generates intermediates that may inhibit active sites for oxygen cleavage [2–8]. The relative occurrence of these two processes is determined by the surface properties of the catalyst. Efficient electrocatalysts are those that reduce oxygen to water at the lowest overpotentials while concomitantly producing the least amount of H_2O_2. Overpotential is important in attaining high power densities in fuel cells [9], while peroxide yield is important from a practical point of view because H_2O_2 production leads to degradation of support materials as well as to the occurrence of corrosion processes, both of which ultimately contribute to a decrease in electrocatalytic efficiency [10].

The ORR continues to be the subject of significant research activity, especially in connection with discovering electrocatalysts that show better activity and which are less expensive and more abundant than Pt-based materials currently used in PEM fuel cells [11–15]. Despite more than a century of effort to identify effective ORR electrocatalysts, the activation overpotential ranges from ≈ 0.3 to 0.45 V, even for Pt, resulting in cathode potentials that deviate significantly from the thermodynamic potential, E^o = 1.23 V *vs* NHE, in acidic solution. Catalyst formulations containing combinations of Pt and of other noble metals with less expensive metals continue to be investigated as possible replacements [16,17]. Pd and Au are known to have very different behavior towards the reduction of molecular oxygen in acidic media. Pd is reported to catalyze

* Corresponding author. Tel.: +575-646-5292; fax: +575-646-2649.
E-mail addresses: jlfernan@fiq.unl.edu.ar (J.L. Fernández), czoski@nmsu.edu (C.G. Zoski).
[1] ISE member.

http://dx.doi.org/10.1016/j.electacta.2015.08.027
0013-4686/

the 4e^- reduction of oxygen to water [18], with the quantity of generated hydrogen peroxide determined by the surface state [19]. It is a noble metal with properties similar to and belonging to the same group of the periodic table as Pt, but is less active for the ORR. However, Pd is less expensive by a factor of three and is about fifty times more abundant [20,21]. Since the earliest report in 2002 demonstrating that Pd alloyed with Pt has ORR activity similar to that of Pt [22], there has been extensive research related to Pd based alloys and core shell structures [23–29]. Modifications in synthesis procedures of both Pd and support structures, as well as the combination of Pd with other metals and oxides, have also been found to enhance Pd ORR activity to a level that compares well with that of Pt [30–39]. Moreover, palladium oxide has been proposed as a constituent of poly-functional catalysts with good performance for oxygen reduction and evolution [40,41].

In contrast, the ORR activity of Au in acid media is much lower, and even when it can be enhanced, it will hardly approach that of Pt and Pd [42]. The more positive standard potential of Au oxidation (E^0 = 1.52 V *vs* NHE) relative to Pt suggests that Au has the capability to perform as a stable and oxide-free metallic cathode electrode [43]. For example, Au alloys, nanoparticles (NPs), and single crystals have all demonstrated enhanced ORR activity [3,4,44–49]. However, since oxygen cleavage is unfavorable on Au, the reaction follows a pathway that enables peroxide intermediates and the production of H_2O_2 as the main reaction product (*i.e.*,2-e^- reduction), even at very negative potentials [50]. In spite of this, it was suggested that the combination of gold with a good oxygen-cleaver metal could lead to a bi-functional catalyst with enhanced performance for the ORR [51]. Additionally, it has been shown that a decrease in the particle size significantly enhances the electrocatalytic activity of Au single NPs for the ORR [52].

Here we report significant effects of synthesis conditions on the overall catalytic activity for the ORR on carbon supported Pd and Au catalysts prepared by an impregnation/oxide precipitation/reduction procedure. More precisely, Pd and Au catalysts composed of NPs dispersed in a partially oxidized environment were prepared by precipitation of hydrated metal oxides followed by chemical, electrochemical or thermal reduction. The extent of oxide reduction was found to strongly affect the performance for the ORR of Pd and Au catalysts as compared to those catalysts prepared from only the metal salt. This effect was first detected by a rapid exploration of catalyst synthesis routes on ORR activity carried out by scanning electrochemical microscopy (SECM) ORR screening on Pd and Au arrays prepared on glassy carbon (GC) substrates [51,53–56]. Metal catalyst spots with different degrees of metal oxidation were generated using rapid array preparation based on dispensing selected reactants on micro-sized circular reaction areas [51,57]. The individual catalyst spots were screened with an ultramicroelectrode (UME) tip to produce a visual color-coded image used to judge the relative efficacy of a given composition. Individual spots were further characterized for the ORR at steady state with the SECM substrate generation-tip collection (SG-TC) mode in a manner similar to rotating ring-disk electrode (RRDE) studies, where the ORR current-potential dependence is locally evaluated on an electrocatalyst spot on the substrate and the tip collects any generated H_2O_2 [58,59]. In SECM, diffusion between the substrate and tip is faster and collection efficiencies are higher compared to the RRDE. Based on the SECM results, traditional RRDE experiments in O_2-saturated sulfuric acid solution were carried out on C/Pd and C/Au prepared at selected conditions which provided results in good agreement with those obtained using SECM. These results, in conjunction with structural and thermal characterization of these catalysts, demonstrate the strong effect that the interactions between Pd and Au and their oxides have on the dispersion and accessible electroactive area of the metals, and on the overall performance for the ORR and provide electrochemical evidence regarding the nature of these interactions.

2. Experimental

2.1. Chemicals and materials

GC plates (1 mm thick, 50 × 50 mm, Alfa Aesar, Ward Hill, MA) were cut into squares (15 × 15 mm). $(NH_4)_2PdCl_4$ (Strems, Newburyport, MA), $HAuCl_4{\cdot}3H_2O$ (Aldrich, Milwaukee, WI), $NaHCO_3$ (Baker, Phillipsburg,NJ), $NaBH_4$ (MP Biomedicals, Solon, OH), glycerol (Fluka, Milwaukee, WI), ethanol (Fisher, Fair Lawn, NJ), Vulcan® XC72R (Cabot Co., Billerica, MA), 5 wt% Nafion® alcoholic solution (Aldrich, Milwaukee,WI), ammonium hydroxide (Fisher, Fair Lawn, NJ) and sulfuric acid (98%, Fisher, Fair Lawn, NJ) were used as received. Reagent solutions were prepared using Milli-Q water (Millipore Co., Bedford, MA). Oxygen and argon gases were ultra-high purity grade.

2.2. Electrodes

Hg/Hg_2SO_4 reference (CH Instruments, Austin, TX) and gold wire counter electrodes were used in all experiments. Gold and platinum UME tips were used in SECM experiments to generate oxygen during the SECM ORR screening (Au) using the tip generation-substrate collection (TG-SC) mode, and in the SG-TC mode (Pt) to oxidize hydrogen peroxide generated by an electrocatalyst spot on a GC substrate. Au and Pt UMEs were constructed by heat-sealing 25 μm diameter (Goodfellow, purity (Au: 99.99%, Pt: 99.9%), temper (hard)) wires in borosilicate glass capillaries under vacuum followed by polishing using 1 μm lapping film (Precision Surfaces International) and 0.3 μm alumina (Micropolish II, Buehler, USA) and sharpening to RG=6 (RG = SECM tip radius/Pt or Au radius). GC plates supporting the catalyst spots served as the substrates. In RRDE experiments, a rotating GC disk (5.61 mm diameter, 0.247 cm^2 surface area) – Pt ring electrode (Pine Model AFE7R9GCPT, Pine Instruments, Grove City, PA) with a maximum collection efficiency of 37% was used. The ring-disk electrode was polished using a 0.3 alumina suspension and sonicated for 10 s to remove alumina before every catalyst deposition.

2.3. Instrumentation

SECM measurements were performed using a PC-controlled CHI model 910B SECM (CH Instruments, Austin, TX) which uses a combination of stepper motors and piezoelectric positioners to control the *x-y-z* displacement. The catalyst arrays supported on GC plates were made using a CHI model 1550 (CH Instruments, Austin, TX) solution dispenser with a piezo-dispenser MicroJet AB-01-60 (MicroFab, Plano, TX). A CH model 760C electrochemical workstation (CH Instruments, Austin, TX) was used in RRDE experiments to control the potentials of both the disk and the ring and to record their currents. In all experiments, the RRDE was rotated at 1000 rpm using a Pine Instruments Analytical Rotator model AFMSRXE (Pine Instruments, Grove City, PA). Thermal treatment of GC plate arrays and carbon supported catalysts were performed using a tube furnace (Lindberg/Blue). XRD spectra were obtained with a Rogaku/Mini Flex II –Desktop X-ray diffractometer using Cu Kα radiation (λ= 1.54059 Å, operated at 40 kV, 250 mA). Thermal analyses were conducted using a Mettler TGA/DSC1 Thermogravimetric Analyzer.

2.4. Preparation of Pd and Au arrays on GC plates

Arrays of Pd catalyst spots (150-200 μm in diameter) supported on GC plates were prepared using a solution dispenser capable of

dispensing picoliter-sized droplets [51,60]. The Pd array contained three rows and six columns of spots, as shown in Scheme S1(A) of the Supplementary Information. The rows were identical to each other and were made to check the reproducibility of the results. Five drops of solution containing 0.13 M $(NH_4)_2PdCl_4$ were dispensed on each spot. This solution was prepared by dissolving the Pd metal salt in a mixture of water and glycerol (2 + 1). Typically, potential pulses with amplitudes of 30 V and pulse periods of 25 μs were applied to eject reproducible single drops of ∼ 100 pL. It should be recognized that the drop volumes for the $NaHCO_3$ and $NaBH_4$ aqueous solutions will be slightly different than that for the metal salts in H_2O/glycerol. This is due to the fact that for a certain value of the pulse potential and time applied to the picodispenser, the volume of the dispensed drop depends on the fluid viscosity. Thus, the dispensed drops of aqueous solutions will have volumes different to the drops of solutions in glycerol/water mixtures. This will be relevant only if a precise calculation of concentration after mixing is required, which is not this case. To produce the precipitation of metal hydrated oxides on selected spots, a solution of 0.2 M $NaHCO_3$ was dispensed on each spot using similar conditions. On some of the spots, varied amounts of 0.1 M $NaBH_4$ solution were dispensed to produce the partial or total reduction of the metal hydrated oxide or of the metal salt. Thus, in the Pd array, 5 drops of $NaHCO_3$ solution were dispensed on columns 1 to 5, and no drop of this solution was dispensed on column 6 so that Pd hydrated oxide precipitated only in columns 1 to 5. An increasing number of $NaBH_4$ solution drops from 0 to 4 were applied on columns 1 to 5 to perform the reduction of Pd hydrated oxide. Four drops of $NaBH_4$ solution were dispensed on the sixth column to reduce the previously dispensed Pd salt that was not converted into the Pd hydrated oxide. The Pd array was thermally treated at 350 °C under argon for 1 h. The Pd hydrated oxides on the array were converted to Pd oxides during thermal treatments [61,62].

In the Au array (Scheme S1(B) of the Supplementary Information), 5 drops of $NaHCO_3$ were dispensed on each spot of columns 2 and 3 in order to precipitate Au hydrated oxide only in those spots. Then, 3 drops of $NaBH_4$ solution were dispensed on columns 3 and 4 to reduce Au hydrated oxide in spot 3 and the Au salt in spot 4. The Au array underwent thermal treatment under hydrogen at 250 °C for 1 hr, on which the Au hydrated oxides on the array were reduced to Au [61,63–65].

2.5. Preparation of a single Pd spot for SECM SG/TC polarization curve measurements

The preparation of a single Pd spot on a GC plate was similar to that of the arrays. Reproducibility was determined in triplicate by making single spots on three separate GC plates. Because every spot on the plate contributes to the electrochemical measurement, it was not possible to look at three spots consecutively on the same GC plate.

2.6. Preparation of C-supported Pd and Au catalysts

Carbon supported Pd catalysts (C/Pd) were prepared on carbon black with a metal loading of 20 wt%. Typically, 32 mg of Vulcan® XC72R was dispersed in 10 mL of a solution of the metal salt (8 mg of metal) in water-ethanol (1:1). This suspension was then agitated ultrasonically for 15 min. To produce the precipitation of Pd hydrated oxide, 3 mL of a 0.2 M $NaHCO_3$ solution was added using a micropipette and the suspension was sonicated for another 15 min. On those catalysts that were reduced using $NaBH_4$, a volume (that varied depending on the metal to reducing agent ratio) of freshly prepared 0.1 M $NaBH_4$ solution was added using a micropipette and the suspension was ultrasonically agitated for 10 min. For the catalysts reported in this work, the ratios between moles of Pd and moles of added $NaBH_4$ were 6.5 (deficient), 2.2 (optimum) and 0.5 (excess), corresponding to the added volumes of 0.1 M $NaBH_4$ solution of 115 μL, 340 μL and 1.5 mL, respectively. The suspensions were left to sit for two hours to allow the solute to sediment. We found that longer sedimentation times led to complete reduction of the hydrated Pd oxide with ethanol. The solid was then separated by centrifugation (12,000 rpm, 20 min) followed by washing steps using water and ethanol. Finally the solid was dispersed in ethanol, poured into a porcelain crucible and dried over a hot plate at about 70 °C. The dried solid was then ground using an Agatha mortar and pestle, placed in a porcelain boat and heated under argon at 350 °C for 1 h in a tube furnace. The Pd hydrated oxides were converted to Pd oxides during thermal treatment in the furnace [62]. Carbon supported Au catalysts (C/Au) were prepared on carbon black with a metal loading of 20 wt% following a similar procedure as described for C/Pd, but applying no heating steps and using solvents with minimum reducing strength. This was done to avoid any possible decomposition of the hydroxide into Au NPs [66]. Typically, 32 mg of Vulcan® XC72R was dispersed in 10 mL of a solution of the metal salt (8 mg of metal) in water. This suspension was then agitated ultrasonically for 30 min. To produce the precipitation of the Au hydrated oxide, 3 mL (an excess to make the solution alkaline) of a 1 M NH_4OH solution was added using a micropipette and the suspension was sonicated for another 15 min. For those catalysts that were reduced using $NaBH_4$, 3 mL of freshly prepared 0.1 M $NaBH_4$ solution was added using a micropipette and the suspension was ultrasonically agitated for 10 min. The added amount of $NaBH_4$ was in excess to completely reduce the Au hydrated oxide. The suspension was left to sit overnight and the solid sediment was then separated by centrifugation followed by washing steps using water and acetone. Finally the solid was dispersed in acetone, poured into a porcelain crucible and dried in a vacuum oven at 35 °C. The dried solid was then ground using an Agatha mortar and pestle, and stored at room temperature. Further treatments that were applied on this material included thermal treatment under argon at 100 °C, 350 °C, and 500 °C for 1 h in a tube furnace. Some of these materials were also heated under hydrogen at 350 °C for 1 h to carry out the reduction of Au hydrated oxide [64,65].

2.7. Preparation of catalyst inks for RRDEs

An ink of the C-supported catalyst (C/Pd or C/Au) was made by dispersing 6 mg in 50 μL of a 5 wt% Nafion® alcoholic solution plus 100 μL of ethanol to obtain a suspension with 0.04 mg catalyst/μL. This suspension was homogenized in an ultrasonic bath for 15 min. A volume of 9.5 μL of this ink was deposited on the 5.61 mm diameter (0.247 cm^2) glassy carbon disk the RRDE. The deposited ink was left to dry in air for 1 min at 35 °C. The metal loading was 6.5 $\mu g/cm^2$. A drop of double deionized water was placed on the deposited ink to avoid over-drying before placing the electrode in the electrochemical cell. The ring-disk electrode was polished using a 0.3 alumina suspension and sonicated for 10 s to remove the alumina before every catalyst deposition.

2.8. Rotating ring-disk experiments

RRDE experiments were performed using a four-electrode cell configuration. RRDE polarization curves were recorded at 1000 rpm in O_2-saturated 0.5 M H_2SO_4 with a constant flow of O_2 (1 atm) through the electrolyte, by linear sweep voltammetry (LSV) scanning the potential in a positive direction at a potential sweep rate of 0.2 mV s^{-1} in the potential range 0.2 V < E_{disk} *vs* NHE < 1.02 V for the C/Pd catalysts and 0.0 V < E_{disk} *vs* NHE < 0.9 V for the C/Au catalysts. During this scan, the potential of the ring was held at 1.1 V *vs* NHE to oxidize hydrogen peroxide formed as a product of the ORR on the disk.

CV activation was performed at 1000 rpm in O_2-saturated 0.5 M H_2SO_4 with a constant flow of O_2 (1 atm) through the electrolyte prior to the RRDE polarization curves by scanning the disk electrode potential at 20 mV s^{-1} while the ring electrode was not polarized. The CV activation was continued until a steady, repetitive CV was obtained.

2.9. SECM experiments

2.9.1. ORR activity screening of catalyst arrays

Au tips were used to generate oxygen during SECM ORR screening using the TG-SC mode, as its shown in Scheme S2(a) in the Supplementary Information. Before starting acquisition of a sequence of SECM images, the tip was polished using 1 μm lapping film and 0.3 μm alumina. Constant tip-current TG-SC measurements were performed by controlling the substrate potential using the SECM bipotentiostat and controlling the tip current using a 9 V battery power source between the tip(positive) and counter electrode [53]. A $Hg/HgSO_4$ reference electrode placed into a sleeve separated from the cell by a leakage-free frit, and a gold wire were used as reference and auxiliary electrodes, respectively. The GC plate supporting the array formed the bottom of a Teflon cell with a 0.7 cm diameter aperture formed by a FETFE o-ring so that the array was exposed to the 0.5 M H_2SO_4 solution. The SECM tip was translated towards the substrate surface using conventional feedback mode SECM, employing the ORR at the SECM tip (E_{Tip} = 0.0 V *vs* NHE) to monitor the approach of the tip to the GC surface through negative feedback. Using the feedback approach curve, the tip-substrate distance was set at 40 μm and the electrolyte solution was then deoxygenated using argon for 15 minutes before starting SECM imaging. A blanket of argon was maintained over the electrolyte solution at all times during the experiment. The SECM tip was scanned in the *x-y* plane at step intervals of 50 μm every 0.2 s, while electrogenerating O_2 from H_2O at constant current. The substrate array potential (E_S) was held at different values where activity for O_2 reduction was detected on some spots. The substrate current (i_S), measured as a function of tip position to produce the SECM image, was larger when the O_2 -generating tip passed over the more active spots. Therefore, the magnitude of the substrate current was used as a direct measure of the electrocatalytic activity of each spot for the ORR.

2.9.2. SG/TC ORR polarization curve activity and H_2O_2 quantification on single spot Pd catalysts

H_2O_2 measurements were carried out in O_2saturated 0.5 M H_2SO_4 acid solution on single spot Pd catalysts supported on a GC plate as shown in Scheme S2(b) in the Supplementary Information [58,59]. The SECM cell configuration was similar to that described in the previous section on ORR SECM screening. A 25 μm diameter Pt UME (RG=6), the collector tip, was positioned 8 μm above the single spot in air saturated 0.5 M H_2SO_4 acid. After positioning the tip, the solution was saturated with O_2; thereafter, an O_2 blanket was kept above the solution. While a LSV of the substrate was recorded from (+) to (-) potentials at a scan rate of 2 mVs^{-1}, the tip, set at a potential of 1.10 V *vs* NHE, simultaneously oxidized hydrogen peroxide generated by the catalytic spot. Tip and substrate background currents were also collected by recording the LSV in argon saturated (i.e., oxygen free) 0.5 M H_2SO_4 solution and subtracted from the total tip and substrate currents recorded.

2.9.3. Characterization

XRD spectra were recorded in the 2θ range $30^\circ \leq 2\theta \leq 90^\circ$ at a scan rate of 3° min^{-1} on approximately 10 mg of C/Pd and C/Au catalysts. Crystalline peaks were analyzed using MDI Jade version 5.0 software. For thermal gravimetric analysis (TGA), the change in weight with temperature for unheated C/Au compositions was measured at a scan rate = 5 °C min^{-1}.

3. Results and discussion

3.1. Chemistry of Pd, Pd(II) oxides, and Au, Au(III) oxides

The precipitation of hydrated Pd(II) oxide, which can be written as $Pd(OH)_2.xH_2O$ or $PdO.nH_2O$, is produced by increasing the pH of a Pd^{2+} solution [62], in our case $PdCl_4^{2-}$, using an alkali such as $NaHCO_3$ (our work) or NaOH. This hydrated oxide can be partially dehydrated to PdO by heating under inert atmosphere up to 500 °C [62]. Reduction of the oxide can be carried out by using H_2 and heating at temperatures greater than 100 °C [61] or by using $NaBH_4$ at room temperature [67].

The precipitation of a gold hydrated oxide from the chloride precursor ($AuCl_3$) is produced by an increase of solution pH using excess $NaHCO_3$ (for the spots in SECM screening) and excess NH_4OH (for the carbon supported catalyst) [63]. It is known that the hydrolysis of Au-Cl bonds and replacement by Au-OH bonds occur when the pH of a gold chloride solution is raised to values larger than around 11. It has been reported that the product is a mixture of non-stoichiometric hydroxides $Au(OH)_x$ that include mainly a hydrated Au(III) oxide $Au_2O_3.nH_2O$ [63,68,69]. We used $NaHCO_3$ on the spots for SECM screening because NH_4OH interacts with the GC support in the areas around the spots and the background current during SECM screening becomes extremely large. By applying a thermal treatment to the Au hydrated oxide at T > 150 °C under inert atmosphere, oxide dehydration should occur [63]. As temperature and/or heating times are increased, the remaining oxide becomes increasingly dehydrated and, in theory, it should be possible to obtain crystalline Au_2O_3[63].

When using ammonium hydroxide to increase pH, one of the products has been reported to be an amino compound of the type $Au(NH_3)_y(H_2O)_z(OH)_3$ [66]. This type of compound decomposes at temperatures around 140 °C, and it is speculated that the NH_3 ligands may reduce some Au(III) cations into Au(0). Thus, we expected that samples treated at T ≥ 140 °C do not contain ammonia ligands, but do contain Au_2O_3 that may be partially hydrated (depending on the temperature) and Au NPs. However, as we show later using XRD, no crystalline gold oxides were detected at any temperature and all Au(III) cations appear to be reduced to Au(0).

Reduction of the hydrated oxide can be produced by applying a reducing agent. Typical reducing agents are H_2 [61] where the reducing strength is regulated by temperature [64,65] and $NaBH_4$ [70] which is a strong reducing agent at room temperature. The partial reduction of hydrated gold oxide can also be performed electrochemically as was also done in this work on Au samples that were not treated thermally.

3.2. SECM ORR screening

Rapid exploration of the effect of synthesis conditions on ORR activity was carried out by SECM ORR screening on Pd and Au arrays prepared on GC substrates as previously reported [53,54]. Briefly, SECM ORR screening in acid solution is based on TG/SC SECM where O_2 produced galvanostatically from H_2O oxidation at the UME tip diffuses to the underlying array where it reacts (Scheme S2(a) in the Supplementary Information). When the tip is close to the array and the catalyst spots are sufficiently far apart, only the spot immediately below the tip is addressed during the array screening [53]. The substrate current, i_S, at that spot at a given potential, E_S, is a measure of the activity of the electrocatalyst spot. Metal catalyst spots with different degrees of metal oxidation were generated using an

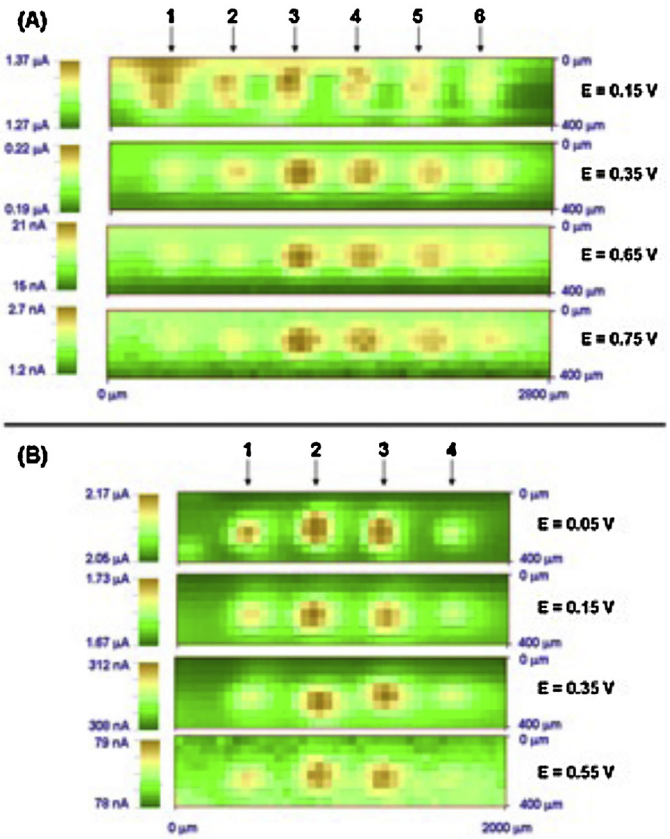

Figure 1. SECM ORR screening of GC/Pd (A) and GC/Au (B) arrays in 0.5 M H_2SO_4. (A) Spots 1 to 5 contain Pd oxide partially reduced with increasing amounts of $NaBH_4$ from left to right. Spot 6 contains Pd from reduction of Pd salt precursor with excess $NaBH_4$. (B) Spots 1 and 4 contain Au from reduction of Au salt using H_2 (1) and excess $NaBH_4/H_2$ (4). Spots 2 and 3 contain Au oxide partially reduced using H_2(2) and excess $NaBH_4/H_2$ (3). All substrate potentials are *vs* NHE.

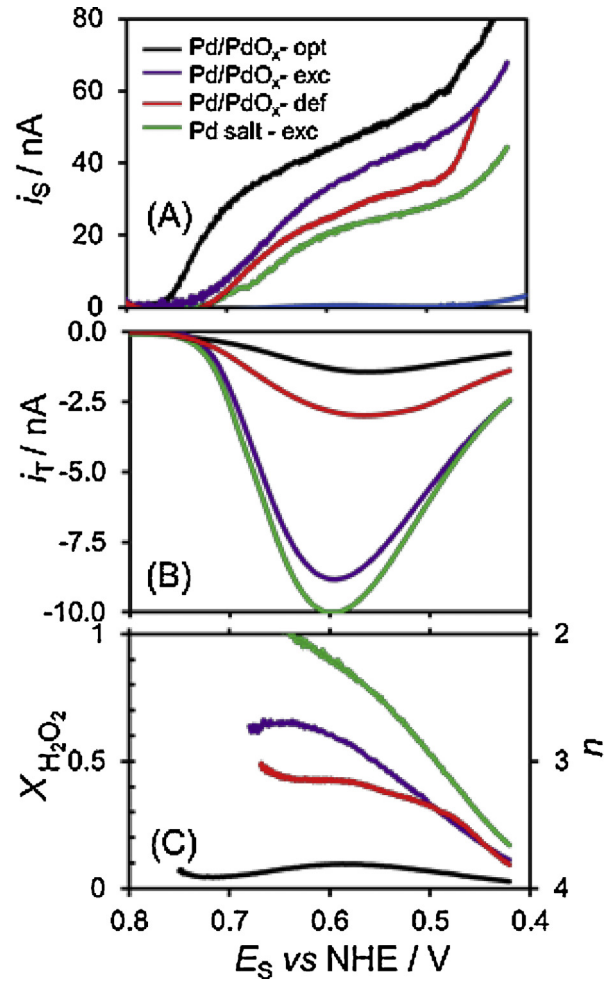

Figure 2. SECM SG/TC investigation of the ORR in O_2 saturated 0.5 M H_2SO_4 at individual Pd/PdO_x spots (A): Reduced with $NaBH_4$: optimum (Pd/PdO_x-opt); excess (Pd/PdO_x-exc); deficient (Pd/PdO_x-def), and Pd salt reduced with excess $NaBH_4$ (Pd salt-exc). (B) H_2O_2 quantification at a Pt tip. (C) H_2O_2 mole fraction and number of electrons. Blue curve in (A) shows the *i-E* behavior of the GC plate in O_2 saturated 0.5 M H_2SO_4. Tip: 25 μm diameter Pt, RG = 6, E_{tip} = 1.10 V *vs* NHE. d = 8 μm (CE_{max} = 60%). Electrocatalyst spots ~100 μm diameter. E_S scanned from + to – at 0.2 mV s^{-1}.

array preparation method that allows the dispensing of selected reactants on circular reaction areas of 150-200 μm in diameter [53]. A constant volume of 500 pL of pure metal precursor solution was dispensed on each spot and the precipitation of the metal hydrated oxide was carried out on some of these spots by localized addition of an excess of sodium bicarbonate solution. An additional chemical reduction step was applied on selected spots by dispensing drops of sodium borohydride solution. Thermal treatments of 350 °C under inert (Ar) or reducing (H_2) conditions were applied on Pd or Au arrays, respectively.

Fig. 1 shows ORR SECM images obtained on a Pd (A) and Au (B) array at different substrate potentials. The color legend corresponds to the electrocatalytic activity of each catalyst spot through its current i_S; brown indicates high activity and green, low activity. At very negative potentials on the Pd array (Fig. 1(A)), the Pd spots show similar ORR currents. At less negative potentials, differences in the ORR currents are observed on spots 1 to 6 that indicate the existence of an optimum range for the added amount of sodium borohydride (spots 3 and 4). These results suggest that the presence of remaining unreduced Pd oxide is beneficial for the ORR performance of Pd catalysts. In the Au array (Fig. 1(B)), the spots generated from precipitation of Au hydrated oxide (spots 2 and 3) show larger ORR currents over the entire potential range, irrespective of the reducing treatment. On the basis of this rapid screening, additional studies, including SECM SG/TC on single Pd spots, RRDE experiments, and characterization using XRD and TGA, were performed in order to understand the effect of oxide precipitation during synthesis of base Pd and Au catalysts on the ORR in acidic media. We present and discuss the results of these experiments in the sections to follow.

3.3. SECM SG/TC on Pd single spots

SECM SG/TC coupled with LSV was carried out in O_2-saturated H_2SO_4 solution on single Pd catalyst spots supported individually on a GC plate [54,58,59]. In this SECM configuration, O_2 is reduced at Pd compositions identified from the SECM ORR screening as E_S is linearly ramped over the ORR potential range. The tip is set at E_T = 1.2 V *vs* NHE in order to oxidize any H_2O_2 produced simultaneously at the substrate through O_2 reduction, as indicated by the substrate and tip reactions (Scheme S2(b) in the Supplementary Information):

$$\text{Substrate}: \quad O_2 + 4H^+ + 4e \rightarrow 2H_2O \quad E^0 = 1.229\,\text{V}\,vs\,\text{NHE} \quad (1)$$

$$O_2 + 2H^+ + 2e \rightarrow H_2O_2 \quad E^0 = 0.67\,\text{V}\,vs\,\text{NHE} \quad (2)$$

$$\text{Tip}: \quad H_2O_2 \rightarrow O_2 + 2H^+ + 2e \quad (3)$$

Fig. 2 shows the ORR LSV (i.e., i_S *vs* E_S) at each single Pd catalyst spot (A), the H_2O_2 collection current at the tip, i_T, (B), the fraction of H_2O_2 collected(C), X_{H2O2}, and the corresponding number of electrons(C), n, as a function of E_S. As shown in Fig. 2(A),

differences in the SG-TC onset potentials for the ORR were found between the spot synthesized with an optimum amount of $NaBH_4$ (*i.e.*, Pd/PdO_x-opt) and those PdO_x compositions based on deficit (*i.e.*, Pd/PdO_x-def) and excess amounts of $NaBH_4$ (*i.e.*, Pd/PdO_x-exc), and the Pd salt reduced with excess $NaBH_4$ (*i.e.*, Pd salt-exc). In good agreement with the SECM results, the activity was larger for those spots synthesized from the hydrated oxide compared to that from only the Pd salt. Significant activity was found on the spots that were reduced with an optimized amount of sodium borohydride, where optimal quantities of metal NPs and metal oxide are believed to co-exist. Fig. 2B demonstrates through i_T (*i.e.*,eq. (3)), that H_2O_2 production during the ORR was smallest for the spot reduced with an optimized amount of sodium borohydride over the entire potential range. These results suggest that the hydrated oxide synthesis route leads to a dispersion of Pd NPs in an oxide environment such that the synergetic effect for the ORR between Pd and its oxide may be related to the inhibition of the peroxide pathway.

The tip and substrate currents were used in calculating n and X_{H2O2} values during the ORR on each catalyst spot, according to the equations [58,59]:

$$n = \frac{4i_S}{\left[i_s + \left|\frac{i_T}{CE_{\max}/100}\right|\right]} = 4\left(1 - \frac{X_{H_2O_2}}{2}\right) \quad (4)$$

$$X_{H_2O_2} = \frac{2\left|\frac{i_T}{CE_{\max}/100}\right|}{\left[i_s + \left|\frac{i_T}{CE_{\max}/100}\right|\right]} = \frac{4-n}{2} \quad (5)$$

where i_T and i_S are the background subtracted tip and substrate currents, respectively. A maximum collection efficiency ($CE_{\max}$) was determined from the following equation [58]:

$$CE_{\max} = A + B\left(\frac{d}{a/b}\right) + C\left(\frac{d}{a/b}\right)^2 + D\left(\frac{d}{a/b}\right)^3 + E\left(\frac{d}{a/b}\right)^4 \quad (6)$$

involving the tip radius (a), substrate (i.e., spot radius) (b), and the tip-substrate distance (d) where the constants A=103.38, B=-2.1681, C=0.02585, D=-1.485 × 10^{-4}, E=3.22 × 10^{-7} for RG=6. For a=12.5 μm, b=50 μm, and d=8 μm, a value of $CE_{\max}$=0.60 (or 60%) is calculated. These parameters were carefully maintained in order to achieve the same collection efficiency on all single catalytic spots studied.

Fig. 2(C) shows the n value variation as a function of the applied substrate potential for the single Pd catalyst spots. In all cases, the calculation of the n value (eq. (4)) is limited by the start of hydrogen adsorption at the catalyst in the less positive potential region. Among the four catalyst spots, the optimum Pd composition (i.e., black curve) produced by reducing precipitated $Pd(OH)_x$ with an optimum quantity of $NaBH_4$ shows an n value closest to the maximum, from n=4 to 3.8, over the entire potential range. For $Pd(OH)_x$ reduced with excess (purple curve) and deficient $NaBH_4$ (red curve), n varied from 3.8 to 3, and 3.8 to 2.7, respectively, depending on the potential. The largest n variation (from 3.6 to near 2) with potential was found for the Pd spot composition obtained by direct reduction of the Pd salt with excess $NaBH_4$ (green curve). Thus, the Pd composition based on PdO_x precipitation followed by partial reduction with an optimum amount of $NaBH_4$ has the lowest H_2O_2 production, and n≈4 over the E_S range indicates that the ORR proceeds mainly through the direct $4e^-$ pathway.

3.4. RRDE polarization curves of C/Pd/PdO_x catalysts

RRDE experiments were carried out in O_2-saturated 0.5 M H_2SO_4 aqueous solution on C/Pd catalysts with varied amounts of Pd oxide. These catalysts were deposited on a GC rotating disk electrode using Nafion as a binder, as described in the Experimental Section.

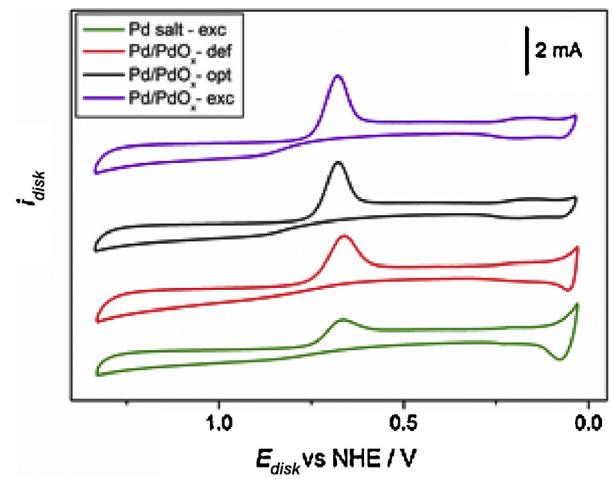

Figure 3. CVs of C/Pd catalysts recorded on the disk of an RRDE at 1000 rpm in O_2 saturated (1 atm) 0.5 M H_2SO_4 at 0.1 Vs^{-1}. C/Pd catalysts were synthesized by precipitation of Pd hydrated oxides using excess $NaHCO_3$ and reduction with optimum (Pd/PdO_x-opt), deficient (Pd/PdO_x-def), and excess $NaBH_4$ (Pd/PdO_x-exc), and reduction of C-impregnated Pd salt with excess $NaBH_4$ (Pd salt-exc). All compositions were heated under Ar at 350°C for 1 hr. The CVs are displaced along the y-axis for better comparison.

Electrochemical pre-treatment of the catalysts was first performed in 0.5 M H_2SO_4 aqueous solution saturated with O_2 (1 atm). The CVs of these C/Pd catalysts at 20 mV/s and at a rotation rate of 1000 rpm are shown in Fig. S1 of the Supplementary Information. Those catalysts synthesized by direct reduction of C-impregnated salt with excess $NaBH_4$ (A) and through the precipitation route and reduced with a deficient amount of $NaBH_4$ (B) quickly reach a steady CV without going through a prolonged transitional period. In contrast, the PdO_x catalyst reduced with optimum (C) and excess amounts of $NaBH_4$(D) required transitional periods in order to reach constant CVs. The CVs show marked differences in the currents for reduction of the anodic oxide that is formed on Pd at E > 0.87 V *vs* NHE. Pd is electro-oxidized at potentials more positive than around 0.87 V *vs* NHE and the anodic oxide is electro-reduced in the negative scan at potentials less positive than ∼ 0.8 V. In these CVs recorded in a solution saturated with oxygen, the oxide reduction current (which shows up as a peak) is overlapped with the oxygen reduction wave. Even with this overlapping, the oxide reduction peak changes from one catalyst to another, as shown more clearly in CVs obtained at a larger scan rate (Fig. 3). These CVs show strong variation of the electrochemically active area of Pd among the different catalysts. More specifically, the compositions prepared following the oxide precipitation route show much larger Pd active areas. This is expected when considering the reported small size and high dispersion of the Pd NPs obtained following this synthesis route [67]. For voltammograms measured in oxygen-free electrolyte for some electrodes (not shown), the oxide reduction peak was almost unchanged with respect to the oxygen-saturated electrolyte (except for the slight shift of the oxygen reduction current). This behavior is reasonable because the anodic limit is sufficiently high to make the metal oxide formation almost insensitive to the presence of dissolved oxygen.

After the stabilization time, a series of ORR polarization curves (Fig. 4) were measured by slow potential scans starting from the negative potential limit (A) and simultaneously monitoring the disk-generated hydrogen peroxide through the oxidation current at the ring (B). Fig. 4(C) shows the number of electrons, n, transferred during the ORR at the disk and the mole fraction of H_2O_2 produced at the disk and detected at the ring electrodes calculated

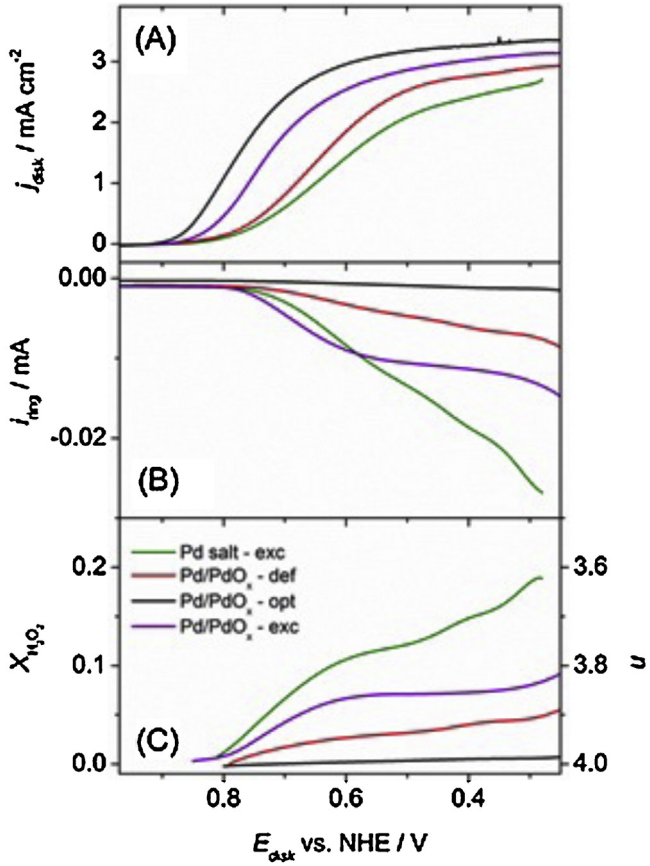

Figure 4. RRDE ORR polarization curves (A) and corresponding ring currents for H_2O_2 oxidation (B), H_2O_2 mole fraction, and number of electrons (C) on C/Pd catalysts synthesized by precipitation of Pd hydrated oxides using excess $NaHCO_3$ and reduction with optimum (Pd/PdO$_x$-opt), deficient (Pd/PdO$_x$-def), and excess $NaBH_4$ (Pd/PdO$_x$-exc), and reduction of C-impregnated Pd salt with $NaBH_4$ (Pd salt-exc). All compositions were heated under Ar at 350°C for 1 hr. Sweep rate = 0.2 mVs^{-1}. E_{ring} = 1.08 V *vs* NHE. Rotation rate = 1000 rpm. Solution: O_2–saturated 0.5 M H_2SO_4.

from the RRDE polarization curves using the following equations [71]:

$$n = \frac{4i_{disk}}{\left[i_{disk} + \left|\frac{i_{ring}}{CE/100}\right|\right]} = 4\left(1 - \frac{X_{H_2O_2}}{2}\right) \quad (7)$$

$$X_{H_2O_2} = \frac{2\left|\frac{i_{ring}}{CE/100}\right|}{\left[i_{disk} + \left|\frac{i_{ring}}{CE/100}\right|\right]} = \frac{4-n}{2} \quad (8)$$

where CE = 37% for the RRDE used in these experiments.

In good agreement with the SECM screening and single spot results, there are differences in the onset potentials for the ORR, in the amount of hydrogen peroxide generated, and in the *n* value during the ORR. The activity was always larger and the amount of hydrogen peroxide generated was less for those catalysts synthesized from reduction of the hydrated oxide compared to those from reduction of the Pd salt. For those catalysts that were partially reduced with deficient and optimum amounts of $NaBH_4$ (*i.e.*, Pd/PdO$_x$-def, Pd/PdO$_x$-opt), the amounts of peroxide detected at the ring were comparatively less than those detected for the catalysts that were completely reduced with excess $NaBH_4$ (*i.e.*, Pd/PdO$_x$-exc, Pd salt-exc). The largest activity and almost null H_2O_2 yield was found on catalysts that were reduced with an optimized amount of sodium borohydride, where optimal quantities of metal particles and metal oxide coexist in the catalyst.

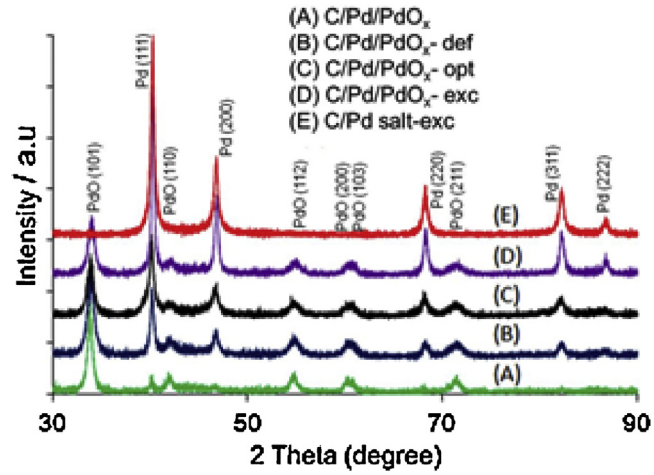

Figure 5. XRD patterns of C/Pd/PdO$_x$ catalysts synthesized by precipitation of Pd hydrated oxides using excess $NaHCO_3$ (A), and reduction with $NaBH_4$: deficient (def) (B), optimum (opt) (C), excess (exc) (D). Reduction of C-impregnated Pd salt with excess $NaBH_4$ is shown as (E). All compositions were heated under Ar at 350 °C for 1 hr. The spectra are displaced along the *y*-axis for comparison.

Fig. 5 shows the X-ray diffraction (XRD) spectra of the C/Pdcatalysts. The C/Pd salt-exc catalyst shows peaks only for the various Pd crystal faces in the spectrum in contrast to the C/PdO$_x$ catalyst which shows peaks only for the PdO crystal faces. The intensity of the Pd and PdO peaks for the C/Pd/PdO$_x$-opt, C/Pd/PdO$_x$-def and C/Pd/PdO$_x$-exc catalysts was found to vary with the amount of $NaBH_4$ added in the synthesis process. In particular, the PdO (101), Pd (111), Pd (200), and Pd (220) peaks were most affected by the quantity of $NaBH_4$ used in the reduction. For example, the $I_{PdO(101)}/I_{Pd(111)}$ ratio was >1 for C/Pd/PdO$_x$-def, ≈ 1 for C/Pd/PdO$_x$-opt, and < 1 for C/Pd/PdO$_x$-exc. The widths of the Pd(220) peaks measured on C/Pd/PdO$_x$-exc (D) and C/Pdsalt-exc (E) catalysts were found to be only barely smaller than those measured on C/Pd/PdO$_x$-def (B) and C/Pd/PdO$_x$-opt (C) catalysts, which may be indicative of slightly larger crystallite sizes. This apparent similarity in crystallite sizes contrasts with the marked differences in the Pd electroactive areas detected by CVs (Fig. 3), and indicates that agglomeration of particles may be important in the catalysts with smaller electroactive areas. The Pd (220) peak is indicative of Pd NPs and increased from C/Pd/PdO$_x$ (A) to C/Pd salt-exc (E) in Fig. 5.

The SECM, RRDE and XRD results suggest that the hydrated oxide synthesis route leads to a lower generation of peroxide during the ORR. This could be caused by the observed increase of the Pd electroactive area inducing a higher consumption of peroxide by a re-adsorption mechanism such as that proposed by Behm et al. [72]. However, the peroxide yield in the Pd electrodes prepared by the hydrated oxide route (which all have about the same area according to the cyclic voltammograms shown in Fig. 3) is very sensitive to the presence of unreduced Pd oxide. Thus, the decrease of the peroxide yield could also be caused by a synergetic interaction between Pd and its oxide. This interaction may be related to the inhibition of the peroxide pathway through the following set of reactions:

$$Pd + \frac{1}{2}O_2 \xrightarrow{PdO_x} PdO_{ad} \quad (9)$$

$$PdO_{ad} + 2e^- + 2H^+ \rightarrow Pd + H_2O \quad (10)$$

where the $4e^-$ pathway is favored following the O_2 cleavage shown in eq. (9) where PdO_{ad} refers to adsorbed PdO. Unreduced PdO could facilitate the $4e^-$ pathway by favoring the occurrence of eq. (9) at the Pd/PdO interface, and by keeping Pd sites free of adsorbed

oxygen inhibitors (i.e., peroxide and superoxide) by removing them through chemical reaction.

Alternatively, the synergetic interaction that produces the decrease in peroxide may be caused by the decomposition of H_2O_2 generated at the Pd surface through the parallel (or peroxide) route (eqs. (11) and (12)) catalyzed by PdO in close proximity to the metal (eq. (13)), producing an effect similar to that observed for a $E_rC'_i$ reaction [73].

$$Pd + O_{2(surface)} + e^- + H^+ \rightarrow PdOOH_{ad} \quad (11)$$

$$PdOOH_{ad} + e^- + H^+ \rightarrow Pd + H_2O_{2(surface)} \quad (12)$$

$$H_2O_{2(surface)} \xrightarrow{PdO_x} \frac{1}{2}O_2 + H_2O \quad (13)$$

Such a synergetic effect is possible through either route when an optimum ratio of metallic Pd and PdO (intrinsically nonconductive) is present in a catalyst where there is intimate contact between both phases without compromising the conductivity and reactant accessibility; this synergetic effect is independent of the nature of the Pd surface atoms.

3.5. RRDE evaluation of C/Au/Au(OH)$_x$ catalysts

Carbon supported Au oxide catalysts deposited on a GC RRDE were electrochemically treated by CV (Fig. S2 in the Supplementary Information) at 1000 rpm in O_2-saturated (1 atm) 0.5 M H_2SO_4 by scanning the potential from 0.98 to 0.03 V *vs* NHE at 20 mV/s. During the synthesis of these catalysts, the decomposition of the chemically precipitated Au hydrated oxide into gold NPs was carefully avoided [66]. The first negative potential scan of those materials that were not thermally treated (Fig. S2(A) of the Supplementary Information), shows a large voltammetric reduction peak after which the gold catalyst layer behaves similarly to those which were reduced using either hydrogen or sodium borohydride (Fig. S2(B),(C), respectively, of the Supplementary Information). This appears to be related to the irreversible electroreduction of Au hydrated oxides in contact with the conductive carbon surface of the C/Au catalysts. Thus, Au NPs dispersed on the carbon support were generated during this first scan from the unreduced Au hydrated oxide in the catalyst layer. This wave was absent in the CVs of C/Au catalysts that were subjected to reducing treatment using either H_2 or sodium borohydride, and on electrodes prepared by direct reduction of metal salts. By applying thermal treatments at different temperatures (35 °C ≤ T ≤ 150 °C) to this material (Fig. S3 in the Supplementary Information), the charge of the first reduction peak decreased due to partial thermal decomposition of the Au hydrated oxide to Au NPs [63] and in theory to Au oxide [66,68,69]; the reduction peak was not detected for T ≥ 150 °C. On all catalysts prepared by this method, a stable CV was reached only after cycling the potential for about three hours, and a shift of the oxygen reduction wave to more positive potentials was observed during this period. The "activation" of these catalysts could be related to an increasing degree of accessibility to the total metal electroactive area in the Nafion-bound catalyst layer as the cycling proceeds and/or to an increasing amount of Au NPs produced by progressive electro-reduction of remaining oxide. After stabilization, the Au electroactive area varied significantly from one catalyst to the other, which was evident from the Au oxide electroreduction peaks of the CVs measured at higher scan rates (Fig. 6). The C/Au catalysts from unreduced Au hydroxide show the largest available electroactive areas.

Fig. 7 shows the XRD spectra for C/Au catalysts that were synthesized by precipitation of Au hydrated oxides using excess NH_4OH and which were either unheated or heated at temperatures of 125, 150, and 350 °C. Upon increasing the temperature, the peak intensities of the Au crystallographic planes in these spectra increase with respect to those registered on the unheated sample (A). In contrast, the widths of the Au peaks were quite similar except for the catalyst treated at 350 °C, where a decrease of the peak width (or an increase of the mean crystallite size) was evident. No Au crystalline oxide peaks were evident in any of the C/Au catalysts that were synthesized, which could be indicative of an amorphous phase. The presence of Au NPs was evident through the Au(220) peak even in the unheated C/Au catalyst. Fig. 8 shows the thermal gravimetric analysis (TGA) of different C/Au catalysts. The as-prepared C/Au(OH)$_x$ sample shows an abrupt weight loss between 165°C and 195°C that can be attributed to the decomposition of amorphous hydrated Au oxide to Au NPs. Similar temperature ranges for the transition from amorphous Au(III) oxides to crystalline Au have been reported [74–76]. The TGA curve for Vulcan carbon, treated identically as in the synthesis of the C/Au(OH)$_x$ sample but without the Au precursor, did not show this abrupt weight loss; the gradual change between 35 to 105 °C can be attributed to moisture evaporation. These curves are parallel to each other after about 200°C, suggesting that the change in weight with temperature is similar. The absence of an abrupt weight loss for C/Au(OH)$_x$ and C/Au-salt reduced with excess $NaBH_4$ suggests the absence of hydrated Au oxide in these samples.

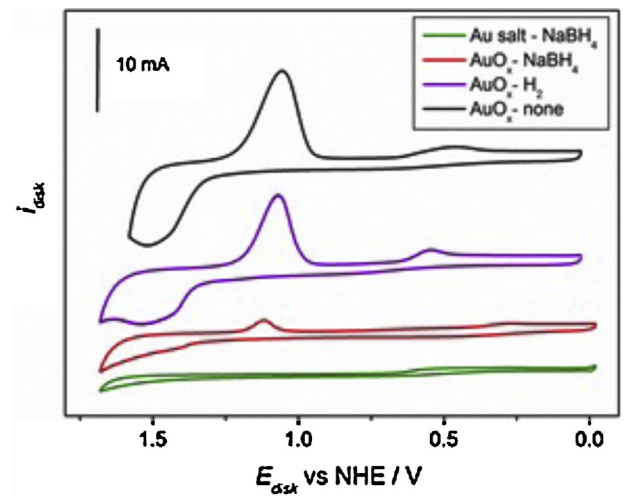

Figure 6. CVs of C/Au catalysts recorded on the disk of an RRDE at 1000 rpm in O_2 saturated (1 atm) 0.5 M H_2SO_4 at 0.1 V s^{-1}. C/Au catalysts were synthesized by reduction of C-impregnated Au salt reduced using $NaBH_4$ (Au salt-$NaBH_4$), by precipitation of Au hydrated oxides with excess NH_4OH and further reduction with $NaBH_4$ (AuO_x-$NaBH_4$) and H_2 at 350 °C (AuO_x–H_2), and without further treatment (AuO_x-none). The CVs are displaced along the *y*-axis for comparison.

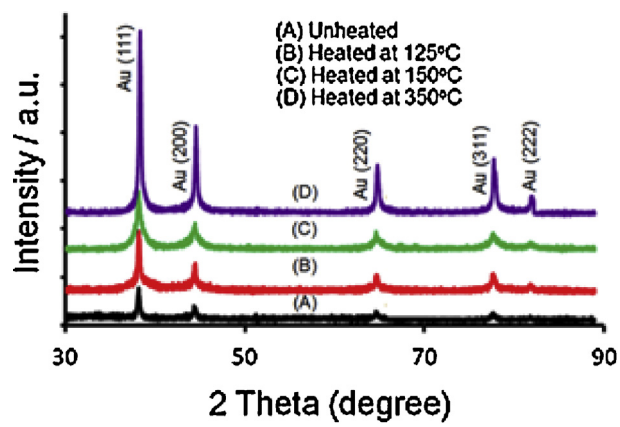

Figure 7. XRD patterns of C/Au catalysts synthesized by precipitation of Au hydrated oxides using excess NH_4OH heated at different temperatures under argon for 1 hr.

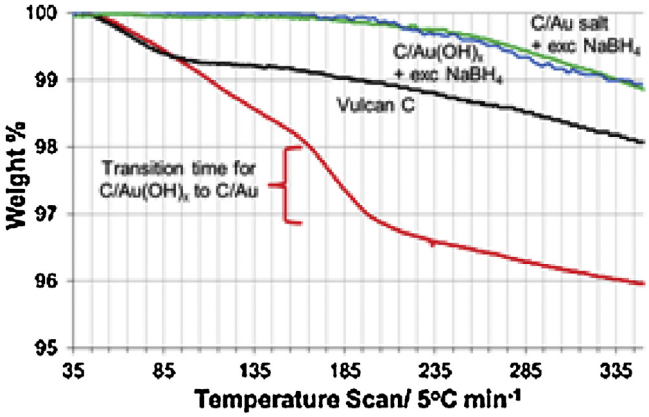

Figure 8. Thermal gravimetric analysis (TGA) of different C/Au catalysts: (1) As prepared C/Au(OH)$_x$ synthesized by precipitation of Au hydrated oxide (red line); (2) C/Au(OH)$_x$ reduced with excess $NaBH_4$ (blue line); (3) C/Au salt reduced with excess $NaBH_4$ (green line). Vulcan carbon was treated following the same synthesis procedure as for C/Au(OH)$_x$, in the absence of the precursor Au salt (black line).

Together, the XRD and TGA analyses indicate that thermal decomposition of the C/Au(OH)$_x$ catalysts results in increased formation of Au NPs with no detectable crystalline Au oxide formation as temperature is increased. The C/Au(OH)$_x$ and C/Au-salt catalysts reduced with excess $NaBH_4$ behave similarly under TGA and do not undergo an abrupt weight loss, indicating the absence of hydrated Au oxide in these samples after chemical reduction. Their similar behavior is also observed during electrochemical activation (Fig. S2 (C), (D) in the Supplementary Information).

3.6. RRDE polarization curves of C/Au/Au(OH)$_x$ catalysts

A series of ORR RRDE polarization curves were measured in O_2-saturated sulfuric acid solution on the catalyst compositions shown in Fig. S2 of the Supplementary Information, after the stabilization time, by slow potential scans starting from the negative potential limit and simultaneously monitoring the disk-generated hydrogen peroxide. Stable ORR curves are shown in Fig. 9 for C/Au. The values of n and X_{H2O2} were calculated from the RRDE polarization curves using eqs. (7) and (8). For all of the C/Au catalysts, the ORR proceeds through the peroxide pathway with significant generation of hydrogen peroxide (Fig. 9(B)). High activity was seen on unreduced C/Au hydrated oxide catalysts, with a shift of the polarization curve to a potential approximately 0.2 V more positive than that measured on the completely reduced catalyst prepared from the Au salt (Fig. 9(A)). In contrast to the C/Pd catalysts, since the C/Au catalysts cannot reduce H_2O_2 over the potential range used experimentally, a larger active area does not lead to a decrease in peroxide yield by re-adsorption. Instead, these observed positive shifts in the ORR and hydrogen peroxide potentials, without a clear decrease in hydrogen peroxide generation, are probably caused by increased dispersion of the Au NPs prepared by the oxide route and the subsequent increase of the accessible Au electroactive area. Such a significant increase in ORR activity that brings reaction (2) almost to a reversible regime has not been observed in any reported study of highly active supported gold NP electrodes [77–80]. Thus, even though the gold material synthesized by this oxide route is not technologically attractive by itself due to the high peroxide yield, it could be an interesting material to combine with other stable catalysts (i.e. oxides or metal complexes) that are capable of efficiently catalyzing the decomposition of H_2O_2.

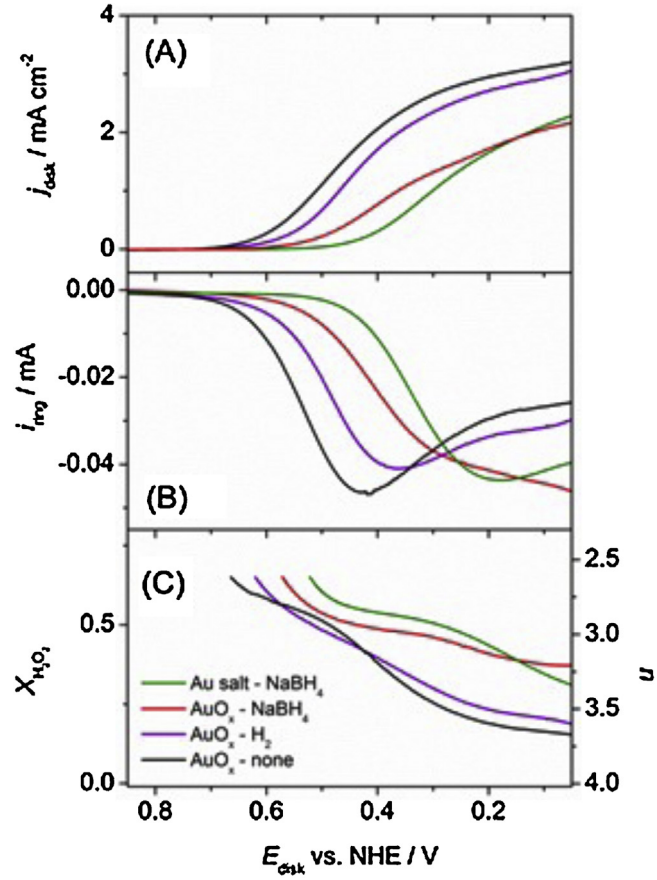

Figure 9. RRDE ORR polarization curves (A) and corresponding ring currents for H_2O_2 oxidation (B), hydrogen peroxide mole fraction, and number of electrons (C) on C/Au catalysts synthesized by reduction of C-impregnated Au salt using $NaBH_4$ (Au salt–$NaBH_4$), by precipitation of Au hydrated oxide without further treatment (AuO_x–none) and with further reduction using H_2 at 350 °C (AuO_x–H_2) and $NaBH_4$ (AuO_x – $NaBH_4$). Sweep rate = 0.2mVs^{-1}. E_{ring} = 1.08 V *vs* NHE. Rotation rate = 1000 rpm. Solution: O_2–saturated 0.5 M H_2SO_4.

4. Conclusions

In this work, we report the preparation via an oxide route of carbon supported Pd and Au electrocatalysts that show a significant enhancement in their overall catalytic activity for the ORR as compared to the same supported metals prepared by usual methods. These enhancements are caused by an oxide-directed higher dispersion of NPs in both metals, and also by metal/metal oxide interactions in carbon supported palladium. Pd and Au catalysts composed of NPs dispersed in a partially oxidized environment were prepared by precipitation of hydrated metal oxides followed by chemical, electrochemical or thermal reduction. The effects that the synthesis through an oxide reduction route has on the overpotential of the ORR by improving the metal NP dispersion and accessibility on Pd and Au catalysts, and on the hydrogen peroxide yield during the ORR on Pd-based catalysts were found to be significant compared to those prepared from only the metal salt.

Rapid exploration of catalyst synthesis routes on ORR activity was carried out by SECM ORR screening on both Pd and Au arrays prepared on GC substrates. For Pd, the SECM ORR screening showed that incomplete reduction of Pd oxide is beneficial for ORR performance of Pd catalysts, and that there is an optimum ratio of metal and metal oxide. SECM was also used to verify that the hydrogen peroxide yield as a secondary product was significantly decreased at these compositions. In the Au array, the spots prepared via a Au

hydrated oxide precipitation showed larger ORR currents over the entire potential range, irrespective of the reducing treatment.

To complement the SECM results, RRDE experiments were carried out in O_2-saturated sulfuric acid solution on C/Pd and C/Au Nafion-embedded catalysts. CV experiments showed that in both C/Pd and C/Au there is a transition time for the response to become stable. A distinct feature of the CVs of C/Pd electrodes is the dependence of the charge on the synthesis conditions for the reduction of Pd oxide that is electrochemically formed at positive potentials, which indicates differences in the resulting Pd electroactive area among the different synthesis methods. It was shown that the electroactive areas of C/Pd electrodes prepared by the oxide reduction route were larger than those prepared from direct reduction. After a stabilization time, ORR polarization curves were measured by slow potential scans with simultaneous monitoring of the disk-generated hydrogen peroxide through the oxidation current at the ring. For C/Pd catalysts, there were significant differences in the required potentials for obtaining a significant ORR current density and in the amount of hydrogen peroxide that was generated (in good agreement with the SECM results). In catalysts where strong reducing treatments were applied (i.e. little or no oxide remaining), the amount of hydrogen peroxide was significant. The current densities at selected potentials were always larger for those catalysts synthesized from the hydrated oxide compared to those from the Pd salt, which was likely caused by the differences in the accessible electroactive areas. For those catalysts that were only partially reduced, the amount of peroxide formed was comparatively less. Significant performance was found on catalysts that were reduced with an optimized amount of sodium borohydride, where optimal quantities of metal particles and metal oxide coexist in the catalyst (as supported by XRD). These results suggest that the hydrated oxide synthesis route leads to a better dispersion of Pd NPs with high electroactive area dispersed in an oxide environment and that there is a synergetic effect for the ORR between Pd and its oxide that prevents hydrogen peroxide production, which may be related to the inhibition of the peroxide pathway and/or to the local decomposition of generated hydrogen peroxide. These results also demonstrate the strong effect that the interactions between Pd and its oxides have on the overall performance of the C/Pd catalysts for the ORR and provide evidence regarding the nature of these interactions. Since these partially oxidized metals are intrinsically very active, they are attractive starting materials for combination with other components with the goal of increasing ORR performance even more through synergetic interactions.

In contrast, the CVs of C/Au catalysts precipitated using ammonium hydroxide showed a large reduction wave in the first negative scan, which appears to be related to the irreversible electroreduction of Au hydrated oxides in contact with the conductive carbon surfaces of the C/Au catalysts. Au NPs highly dispersed on the carbon support were generated during this first scan. This wave was absent in the CVs of C/Au catalysts that were subjected to reducing treatment using either H_2 or sodium borohydride, and on catalysts prepared by direct reduction of metal salts. The catalysts resulting from electrochemical reduction of precipitated gold oxides showed much larger Au electroactive areas, as demonstrated by the higher charges for electroformed oxide reduction measured from the CVs. For all of the C/Au catalysts, the reaction proceeds through the peroxide pathway with generation of hydrogen peroxide. Significant activity was found on unreduced C/Au hydrated oxide catalysts, with polarization curves that closely approach reversible behavior, shifted approximately 0.2 V more positive than those measured on the completely reduced catalyst prepared from the Au salt. This shift in the polarization curves may be related to a much larger available Au electroactive area, and suggests that these catalysts could be interesting base materials in combination with efficient peroxide decomposers to fabricate bi-functional Au-based catalysts for the electroreduction of oxygen to water. These investigations are underway in this laboratory.

Acknowledgements

This work was funded by the National Science Foundation (CHE-1408608, CHE-0809966, C.G.Z.) and a travel grant to J.L.F. by CONICET (Argentina).

Appendix A. Supplementary data

Supplementary data associated with this article can be found, in the online version, at http://dx.doi.org/10.1016/j.electacta.2015.08.027.

References

[1] K. Kinoshita, Electrochemical Oxygen Technology, John Wiley & Sons, New York, 1992.
[2] R. Adžić, in: J. Lipkowski, P.N. Ross (Eds.), Electrocatalysis, Ch. 5, Wiley-VCH, N.Y, 1998, pp. 197–242.
[3] N. Ohta, K. Nomura, I. Yagi, Adsorption and Electroreduction of Oxygen on Gold in Acidic Media: in Situ Spectroscopic Identification of Adsorbed Molecular Oxygen and Hydrogen Superoxide, J. Phys. Chem. C 116 (2012) 14390–14400.
[4] G. Li, R. Jin, Atomically Precise Gold Nanoclusters as New Model Catalysts, Acct. Chem. Res. 46 (2013) 1749–1758.
[5] Q. Fu, F. Yang, X. Bao, Interface-Confined Oxide Nanostructures for Catalytic Oxidation Reactions, Acct. Chem. Res. 46 (2013) 1692–1701.
[6] S. Zhang, L. Nguyen, Y. Zhu, S. Zhan, C.-K. Tsung, F. Tao, In-Situ Studies of Nanocatalysis, Acct. Chem. Res. 46 (2013) 1731–1739.
[7] S. Schauermann, N. Nilius, S. Shaikhutdinov, H.-K. Freund, Nanoparticles for Heterogneous Catalysis: New Mechanistic Insights, Acct. Chem. Res. 46 (2013) 1673–1681.
[8] H. Zhang, M. Jin, Y. Xiong, B. Lim, Y. Xia, Shape-Controlled Synthesis of Pd Nanocrystals and Their Catalytic Applications, Acct. Chem. Res. 46 (2013) 1783–1794.
[9] L. Carrette, K.A. Friedrich, U. Stimming, Fuel Cells – Fundamental and Applications, Fuel Cells 1 (2001) 5–38.
[10] B. Bittins-Cattaneo, S. Wasmus, B. Lopez-Mishima, W. Vielstich, Reduction of oxygen in an acidic methanol/oxygen (air) fuel cell: an online MS study, J. Appl. Electrochem. 23 (1993) 625–630.
[11] J. Wu, H. Yang, Platinum-Based Oxygen Reduction Electrocatalysts, Acct. Chem. Res. 46 (2013) 1848–1857.
[12] G. Wu, P. Zelenay, Nanostructured Nonprecious Metal Catalysts for Oxygen Reduction Reaction, Acct. Chem. Res. 46 (2013) 1878–1889.
[13] M. Uchida, Y.-C. Park, K. Kakinuma, H. Yano, D.A. Tryk, T. Kamino, H. Uchida, M. Watanabe, Effect of the State of Distribution of Supported Pt Nanoparticles on Effective Pt Utilization in Polymer Electrolyte Fuel Cells, Phys. Chem. Chem. Phys. 15 (2013) 11236–11247.
[14] A. Rabis, P. Rodriguez, T.J. Schmidt, Electrocatalysts for Polymer Electrolyte Fuel Cells: Recent Achievements and Future Challenges, ACS Catal. 2 (2012) 864–890.
[15] Z. Chen, D. Higgins, A. Yu, L. Zhang, J. Zhang, A Review on Non-Precious Metal Electrocatalysts for PEM Fuel Cells, Energy Environ. Sci. 4 (2011) 3167–3192.
[16] A.A. Gewirth, M.S. Thorum, Electroreduction of Dioxygen for Fuel-Cell Applications: Materials and Challenges, Inorg. Chem. 152 (2010) 3557–3566.
[17] B. Wang, Recent development of non-platinum catalysts for oxygen reduction reaction, J. Power. Sources 152 (2005) 1–5.
[18] M. Shao, Palladium-based electrocatalysts for hydrogen oxidation and oxygen reduction reactions, J. Power Sources 196 (2011) 2433–2444.
[19] T.R. Blackburn, J.J. Lingane, A study of the chronopotentiometric reductions of oxygen and hydrogen peroxide at a palladium electrode, J. Electroanal. Chem. 5 (1963) 216–235.
[20] E. Antolini, Palladium in Fuel Cell Catalysis, Energy Environ. Sci. 2 (2009) 915–931.
[21] E. Antolini, S.C. Zignani, S.F. Santos, E.R. Gonzalez, Palladium-Based Electrodes: A Way to Reduce Platinum Content in Polymer Electrolyte Membrane Fuel Cells, Electrochim. Acta 56 (2011) 2299–2305.
[22] M.J. Escudero, E. Hontanon, S. Schwartz, M. Boutonnet, L. Daza, Development and performance characterization of new electrocatalysts for PEMFC, J. Power Sources 106 (2002) 206–214.
[23] V. Raghuveer, P.J. Ferreira, A. Manthiram, Comparison of Pd–Co–Au electrocatalysts prepared by conventional borohydride and microemulsion methods for oxygen reduction in fuel cells, Electrochem. Commun. 8 (2006) 807–814.
[24] Y. Gao, G. Wang, B. Wu, C. Deng, Y. Gao, Highly active carbon-supported PdNi catalyst for formic acid electrooxidation, J. Appl. Electrochem. 41 (2011) 1–6.
[25] M. Shao, P. Liu, J. Zhang, R.R. Adzic, Origin of Enhanced Activity in Palladium Alloy Electrocatalaysts for Oxygen Reduction Reaction, J. Phys. Chem. B 111 (2007) 6772–6775.

[26] W. Mustain, K. Keith, J. Prakash, $CoPd_x$ oxygen reduction electrocatalysts for polymer electrolyte membrane and direct methanol fuel cells, Electrochim. Acta. 52 (2007) 2102–2108.
[27] O. Savadogo, K. Lee, K. Oishi, S. Mitsushima, N. Kamiya, K.I. Ota, New palladium alloys catalyst for the oxygen reduction reaction in an acid medium, Electrochem. Commun. 6 (2004) 105–109.
[28] W.P. Zhou, M.B. Vukmirovic, K. Sasaki, R.R. Adzic, Oxygen reduction reaction on a Pt monolayer on a Pd $_2$Co(111) single crystal surface, ECS Trans. 13 (2008) 23–28.
[29] M.H. Shao, T. Huang, P. Liu, J. Zhang, K. Sasaki, M.B. Vukmirovic, R.R. Adzic, Palladium monolayer and palladium alloy electrocatalysts for oxygen reduction, Langmuir 22 (2006) 10409–10415.
[30] Y. Liang, Z. Mengang, M. Juan, Y. Tang, Y. Chen, T. Lu, Highly dispersed carbon-supported Pd nanoparticles catalyst synthesized by novel precipitation–reduction method for formic acid electrooxidation, Electrochim. Acta. 56 (2011) 4696–4702.
[31] L. Xiao, L. Zhuang, Y. Liu, J. Lu, H.D. Abruña, Activating Pd by Morphology Tailoring for Oxygen Reduction, J. Am. Chem. Soc. 131 (2009) 602–608.
[32] Z. Yan, H. Meng, L. Shi, Z. Li, P.K. Shen, Synthesis of mesoporous hollow carbon hemispheres as highly efficient Pd electrocatalyst support for ethanol oxidation, Electrochem. Commun. 12 (2010) 689–692.
[33] G. Ramos-Sánchez, M.M. Bruno, Y.R.J. Thomas, H.R. Corti, O. Solorza-Feria, Mesoporous carbon supported nanoparticulated $PdNi_2$: A methanol tolerant oxygen reduction electrocatalyst, Int. J. Hydrogen Energy 37 (2012) 31–40.
[34] Z. Yan, G. He, G. Zhang, H. Meng, P. Shen, Pd nanoparticles supported on ultra-high surface area honeycomb-like carbon for alcohol electrooxidation, Int. J. Hydrogen Energy 35 (2010) 3263–3269.
[35] W. Ye, H. Hu, H. Zhang, F. Zhou, W. Liu, Multi-walled carbon nanotube supported Pd and Pt nanoparticles with high solution affinity for effective electrocatalysis, Applied Surface Science 256 (2010) 6723–6728.
[36] K. Jukk, N. Alexeyeva, C. Johans, K. Kontturi, K. Tammeveski, Oxygen reduction on Pd nanoparticle/multi-walled carbon nanotube composites, J. Electroanal. Chem. 666 (2012) 67–75.
[37] R. Rego, M.C. Oliveira, F. Alcaide, G. Álvarez, Development of a carbon paper-supported Pd catalyst for PEMFC application, Int. J. Hydrogen Energy 37 (2012) 7191–7199.
[38] V. Di Noto, E. Negro, S. Polizzi, P. Riello, P. Atanassov, Preparation, characterization and single-cell performance of a new class of Pd-carbon nitride electrocatalysts for oxygen reduction reaction in PEMFCs, Appl, Catal. B 111–112 (2012) 185–199.
[39] M. Arenz, T.J. Schmidt, K. Wandelt, P.N. Ross, N.M. Markovic, The Oxygen Reduction Reaction on Thin Palladium Films Supported on a Pt(111) Electrode, J. Phys. Chem. B 107 (2003) 9813–9819.
[40] J. Sunarso, A.M. Glushenkov, A.A.J. Torriero, P.C. Howlett, Y. Chen, D.R. MacFarlane, M. Forsyth, Bi-functional water/oxygen electrocatalyst based on PdO-RuO_2 composites, J. Electrochem. Soc. 160 (2013) H74–H79.
[41] Q. Wu, Z. Rao, L. Yuan, L. Jiang, G. Sun, J. Ruan, Z. Zhou, S. Sang, Carbon supported PdO with improved activity and stability for oxygen reduction reaction in alkaline solution, Electrochim. Acta 150 (2014) 157–166.
[42] C. Wang, D. Vliet, K.L. More, N.J. Zaluzec, S. Peng, S. Sun, H. Daimon, G. Wang, J. Greeley, J. Pearson, A.P. Paulikas, G. Karapetrov, D. Strmcnik, N.M. Markovic, V.R. Stamenkovic, Multimetallic Au/$FePt_3$ nanoparticles as highly durable electrocatalyst, Nano Lett. 11 (2011) 919–926.
[43] Standard Potentials in Aqueous Solution, A.J. Bard, P.T. Parsons, J. Jordan (Eds.), Ch. 11, Marcel Dekker, Inc., New York and Basel, 1985, p. 319.
[44] Y. Park, S. Nam, Y. Oh, H. Choi, J. Park, B. Park, Electrochemical promotion of oxygen reduction on gold with aluminum phosphate overlayer, J. Phys. Chem. C 115 (2011) 7092–7096.
[45] J. Zhang, F.H.B. Lima, M.H. Shao, K. Sasaki, J.X. Wang, J. Hanson, R.R. Adzic, Platinum monolayer on non-noble metal-noble metal core-shell nanoparticle electrocatalysts for O_2 reduction, J. Phys. Chem. B 109 (2005) 22701–22704.
[46] Y. Lu, Z. Xu, H.A. Gasteiger, S. Chen, K. Hamad-Schifferli, Y. Shao-Horn, Platinum-gold nanoparticles: a highly active bifunctionalelectrocatalyst for rechargeable lithium-air batteries, J. Am. Chem. Soc. 132 (2010) 12170–12171.
[47] I. Yagi, T. Ishida, K. Uosaki, Electrocatalytic reduction of oxygen to water at Au nanoclusters vacuum-evaporated on boron-doped diamond in acidic solution, Electrochem. Commun. 6 (2004) 773–779.
[48] F. Gao, M.S. El-Deab, T. Okajima, T. Ohsaka, Electrochemical preparation of a Au crystal with peculiar morphology and unique growth orientation and its catalysis for oxygen reduction, J. Elecrochem. Soc. 152 (2005) A1226–A1232.
[49] R.R. Adzic, S. Strbac, N. Anastasijevic, Electrocatalysis of oxygen on single crystal gold electrodes, Mater. Chem. Phys. 22 (1989) 349–375.
[50] M.A. Genshaw, A. Damjanovic, J. O'MBockris, Hydrogen peroxide formation in oxygen reduction at gold electrodes. I. Acid solution, J. Electroanal. Chem. 9 (1967) 163–172.
[51] J.L. Fernández, D.A. Walsh, A.J. Bard, Thermodynamic Guidelines for the Design of Bimetallic Catalysts for Oxygen Reduction and Rapid Screening by Scanning Electrochemical Microscopy, J. Am. Chem. Soc. 127 (2005) 357–365.
[52] Y. Li, J.T. Cox, B. Zhang, Electrochemical Responses and Electrocatalysis at Single Au Nanoparticles, J. Am. Chem. Soc. 132 (2010) 3047–3054.
[53] J.L. Fernández, A.J. Bard, Scanning Electrochemical Microscopy. 47. Imaging Electrocatalytic Activity for Oxygen Reduction in an Acidic Medium by the Tip Generation-Substrate Collection Mode, Anal. Chem. 75 (2003) 2967–2974.
[54] J. Rodriguez-Lopez, C.G. Zoski, A.J. Bard, Application to Electrocatalysis and Photocatalysis and Surface Interrogation, in: A.J. Bard, M.V. Mirkin (Eds.), Scanning Electrochemical Microscopy, 2nd ed., CH16, Taylor and Francis, N.Y., 2012, pp. 525–568.
[55] S. Amemiya, A.J. Bard, F.-R.F. Fan, M.V. Mirkin, P.R. Unwin, Scanning Electrochemical Microscopy, Annu. Rev. Anal. Chem. 1 (2008) 95–131.
[56] F.-R.F. Fan, J. Fernandez, B. Liu, J. Mauzeroll, Scanning Electrochemical Microscopy, in: C.G. Zoski (Ed.), Handbook of Electrochemistry, Ch. 12, Elsevier, Amsterdam, 2007, pp. 471–540.
[57] W. Li, F-R.F. Fan, A.J. Bard, The Application of Scanning Electrochemical Microscopy to the Discovery of Pd-W Electrocatalysts for the Oxygen Reduction Reaction that Demonstrate High Activity, Stability, and Methanol Tolerance, J. Solid State Electrochem. 16 (2012) 2563–2568.
[58] C.M. Sánchez-Sánchez, J. Rodriguez-López, A.J. Bard, Scanning Electrochemical Microscopy. 60. Quantitative Calibration of the SECM Substrate Generation/Tip Collection Mode and its Use for the Study of the Oxygen Reduction Mechanism, Anal. Chem. 80 (2008) 3254–3260.
[59] C.M. Sánchez-Sánchez, A.J. Bard, Hydrogen Peroxide Production in the Oxygen Reduction Reaction at Different Electrocatalysts as Quantified by Scanning Electrochemical Microscopy, Anal. Chem. 81 (2009) 8094–8100.
[60] J.L. Fernández, N. Mano, A. Heller, A.J. Bard, Optimization of Wired Enzyme O_2-Electroreduction Catalyst Compositions by Scanning Electrochemical Microscopy, Angew. Chem. Int. Ed. 43 (2004) 6355–6357.
[61] R.L. Moss, Preparation and Characterization of Supported Metal Catalysts, in: R.B. Anderson, P.T. Dawson (Eds.), Experimental Methods in Catalytic Research, Vol. 2, Ch. 2, Academic Press, New York, 1976, p. 43.
[62] S.E. Livingstone, The Second and Third Row Elements of Group VIII A, B and C, in: A.F. Trotman-Dickenson (Ed.), Comprehensive Inorganic Chemistry, Vol. 3, Ch. 43, Pergamon Press, Oxford, 1973, p. 1163.
[63] B.F.G. Johnson, R. Davis, Gold, in: A.F. Trotman-Dickenson (Ed.), Comprehensive Inorganic Chemistry, Vol. 3, Ch. 29, Pergamon Press, Oxford, 1973, p. 129.
[64] J.H. Yang, J.D. Henao, C. Costello, M.C. Kung, H.H. Kung, J.T. Miller, A.J. Kropf, J.-G. Kim, J.R. Regalbuto, M.T. Bore, H.N. Pham, A.K. Datye, J.D. Laeger, K. Kharas, Understanding preparation variables in the synthesis of Au/Al $_2O_3$ using EXAFS and electron microscopy, Appl. Catal. A 291 (2005) 73–84.
[65] S.-H. Wu, X.-C. Zheng, S.-R. Wang, D.-Z. Han, W.-P. Huang, S.-M. Zhang, TiO_2 supported nano - Au catalysts prepared via solvated metal atom impregnation for low-temperature CO oxidation, Catal. Letters 97 (2004) 17–23.
[66] L. Delannoy, N. El Hassan, A. Musi, N.N. Le To, J.-M. Krafft, C. Louis, Preparation of supported gold nanoparticles by a modified incipient wetness impregnation method, J. Phys. Chem. B 110 (2006) 22471–22478.
[67] T. Harada, S. Ikeda, M. Miyazaki, T. Sakata, H. Mori, M. Matsumura, A simple method for preparing highly active palladium catalysts loaded on various carbon supports for liquid-phase oxidation and hydrogenation reactions, J. Mol. Catal. A: Chem. 268 (2007) 59–64.
[68] S. Ivanova, C. Petit, V. Pitchon, A new preparation method for the formation of gold nanoparticles on an oxide support, Appl. Catal. A 267 (2004) 191–201.
[69] C.-K. Chang, Y.-J. Cheng, C.-T. Yeh, Characterizations of alumina-supported gold with temperature-programmed reduction, Appl. Catal. A 174 (1998) 13–23.
[70] Y. Liu, K.B. Male, P. Bouvrette, J.H.T. Luong, Control of the Size and Distribution of Gold Nanoparticles by Unmodified Cyclodextrins, Chem. Mater. 15 (2003) 4172–4180.
[71] R.K. Singh, R. Rahul, M. Neergat, Stability Issues in Pd-Based Catalysts: The Role of Surface Pt in Improving the Stability and Oxygen Reduction Reaction (ORR) Activity, Phys. Chem. Chem. Phys. 15 (2013) 13044–13051.
[72] A. Schneider, L. Colmenares, Y.E. Seidel, Z. Jusys, B. Wickman, B. Kasemo, R.J. Behm, Transport effects in the oxygen reduction reaction on nanostructured, planar glassy carbon supported Pt/GC model electrodes", Phys, Chem. Chem. Phys. 10 (2008) 1931–1943.
[73] A.J. Bard, L.R. Faulkner, Electrochemical Methods, 2nd Ed., Wiley, New York, 2001, pp. 471–533.
[74] P. Patnaik, Handbook of Inorganic Chemicals, McGraw-Hill Press, New York, 2003.
[75] B.F.G. Johnson, R. Davis, in: A.F. Trotman-Dickenson (Ed.), Comprehensive Inorganic Chemistry, Pergamon Press, Oxford, 1973.
[76] H. Tsai, E. Hu, K. Perng, M. Chen, J. Wu, Y. Chang, Instability of gold oxide Au_2O_3, Surf. Sci. 537 (2003) L447–L450.
[77] N. Alexeyeva, T. Laaksonen, K. Kontturi, F. Mirkhalaf, D.J. Schiffrin, K. Tammeveski, Oxygen reduction on gold nanoparticle/multi-walled carbon nanotubes modified glassy carbon electrodes in acid solution, Electrochem. Commun. 8 (2006) 1475–1480.
[78] M.S. El- Deab, T. Ohsaka, An extraordinary electrocatalytic reduction of oxygen on gold nanoparticles-electrodeposited gold electrodes, Electrochem. Commun. 4 (2002) 288–292.
[79] M.S. El- Deab, T. Ohsaka, Hydrodynamic voltammetric studies of the oxygen reduction at gold nanoparticles-electrodeposited gold electrodes, Electrochim. Acta 47 (2002) 4255–4261.
[80] S. Guerin, B.E. Hayden, D. Pletcher, M.E. Rendall, J.-P. Suchsland, A combinatorial approach to the study of particle size effects on supported electrocatalysts: Oxygen reduction on gold, J. Comb. Chem. 8 (2006) 679–686.